Journal Pre-proofs

Using Proton Nuclear Magnetic Resonance (NMR) as a calibrating reference for magnetic field measurement instruments: sensitive volume and magnetic field homogeneity

Gonzalo G. Rodriguez, Guillermo Forte, Esteban Anoardo

PII: S0263-2241(19)31093-0
DOI: https://doi.org/10.1016/j.measurement.2019.107228
Reference: MEASUR 107228

To appear in: *Measurement*

Received Date: 11 September 2019
Revised Date: 22 October 2019
Accepted Date: 30 October 2019

Please cite this article as: G.G. Rodriguez, G. Forte, E. Anoardo, Using Proton Nuclear Magnetic Resonance (NMR) as a calibrating reference for magnetic field measurement instruments: sensitive volume and magnetic field homogeneity, *Measurement* (2019), doi: https://doi.org/10.1016/j.measurement.2019.107228

Using Proton Nuclear Magnetic Resonance (NMR) as a calibrating reference for magnetic field measurement instruments: sensitive volume and magnetic field homogeneity

Gonzalo G. Rodriguez[1], Guillermo Forte[1,2] and Esteban Anoardo[1,2]*

1 Laboratorio de Relaxometría y Técnicas Especiales (LaRTE), Grupo de Resonancia Magnética Nuclear. FaMAF - Universidad Nacional de Córdoba and IFEG-CONICET.
2 Trovintek Advanced Magnetic Systems.
Córdoba, Argentina.

Keywords: NMR, metrology, magnetic field measurement, magnetic field compensation.

*Corresponding Author: Esteban Anoardo, **anoardo@famaf.unc.edu.ar**

Abstract

Nuclear magnetic resonance can be conveniently used to set up reference values of magnetic flux densities for the calibration of measurement instrumentation. Two measurement procedures are proposed based on the Fourier analysis of the nuclear magnetic signal. Particularly, we consider the situation where the reference magnetic flux density may change its value across the sensor active area/volume due to spatial inhomogeneities. An explored potential solution uses an electronic compensation system in order to minimize the spatial inhomogeneities of the magnetic flux density within the calibrating volume. For this purpose, a previously designed device was added to the magnetic resonance apparatus. Both methods allow a performance better than 10 ppm in calibrating measurements by using a magnetic flux density source of the order of 100 ppm in spatial homogeneity within the calibrating volume. Examples of both methods are discussed.

INTRODUCTION

Helmholtz coils (HC) are commonly used as magnetic flux density standards in magnetic metrology. The magnetic flux density becomes defined by the coil current, coil dimensions and its number of turns [1-4]. HC have an intrinsic uncertainty due to constructive imperfections [5,6]. A further spurious aspect attains to the magnetic field inhomogeneity which increases abruptly as the spatial position goes outside the azimuthal symmetry axis. Consequently, it turns out that it is only possible to produce a calibrating field with good accuracy within a cylindrical volume that is restricted to the proximities of the symmetry axis, and only limited to a length that is usually shorter than the coil radius. In the practice, this limits the use of HC calibrations to small sensors, unless larger coils are used (which may be associated to larger currents). Another feature to consider is that large magnetic flux densities are difficult to reach in this way. Consequently, the use of HC for calibrations is only viable to sensors with small active sensing area and operating at low magnetic fields.

The use of Nuclear Magnetic Resonance (NMR) instruments as primary standards or calibrating references [7-12] is based on the simple linear relationship between the Larmor frequency (precession frequency of the nuclear magnetization) and the magnetic flux density [13]. In this method, magnetic flux density measurements are translated to frequency measurements [14-17]. Since frequency (and time) is one of the most accurately measured physical quantities [18], NMR turns into a highly attractive technique for metrological use. Oftentimes though, it is considered one of the most accurate standards for measuring static (DC) magnetic flux densities [19,20]. The procedure, however, is not quite as straightforward as one might think. The purpose of analyzing this option in a greater detail was essentially supported by the relative simplicity of the involved hardware, and the possibility to set-up high performance standards at moderate/low costs.

We start the manuscript by briefly explaining the background concepts and establishing the measurement model. Then we define the measurand and present two different experimental procedures (“indirect” and “direct” methods). Both methods are based on the analysis of the Fourier Transform of the NMR signal. The indirect method allows treating transformed signals without any additional hardware. In contrast, the direct method is supported by additional hardware for the compensation of spatial inhomogeneities of the magnetic flux density generated by the used electromagnet. In this case, the transformed signal turns out to be a symmetric-like distribution. Finally, both methods are compared.

Theoretical framework

a) Measurement principle

In order to quantify all mayor sources of uncertainty it is necessary to use a very well-know phenomenon. It is also desirable to cover the widest possible range of the magnitude to be measured using the same principle. The range of our interest (50 - 500 mT) can conveniently be handled using an electromagnet-based NMR instrument. This approach has the advantage that different calibrating points can be adjusted using the same hardware, by just installing specific probes that are tuned and optimized at the selected Larmor frequency values. The technique has been used since the 40's [21,22] and turned to be a very well-know and robust procedure [13,23]. Because of its resonance characteristic and the equivalence of magnetic flux density in Larmor frequency units, NMR is a very sensitive and selective technique which enables magnetic flux measurements with great precision [14-17,19,24]. The technique can be used to measure flux densities of values from the order of the earth magnetic field up to several Teslas.

b) Measurement model

Many atomic nuclei in their ground state have a non-zero spin angular momentum $I\hbar$ and dipole magnetic moment $M = \gamma\hbar I$ collinear with it. These moments are the responsible for the nuclear magnetism. According to the classical theory of electromagnetism, in the presence of an external magnetic flux density B, each nucleus precesses with a Larmor frequency $\omega = -\gamma B$, where γ is the nuclear gyromagnetic ratio [13]. The observed NMR signal originates in the precession of the macroscopic magnetization that builds-up from the superposition of all the nuclear magnetic moments. Strictly speaking, each nucleus sees a different magnetic flux density and, therefore, precesses at a different frequency. This difference in precession frequency between nuclei depends on many factors such as nuclear and electron interactions, change in magnetic susceptibility across the sample and spatial inhomogeneities of the magnetic flux density. As a consequence, the NMR signal contains different frequency components associated to different isocromats (nuclei whose precession occur at the same frequency). Therefore, as the macroscopic magnetization undergoes a precession in the magnetic flux density to be measured, the coherence loss between different isocromats provokes a decay of the NMR signal (or FID, free induction decay) amplitude. In addition, the signal decay is associated to the spin-spin (T_2) and spin-lattice (T_1) relaxation processes [13].

For a typical experiment, the signal decay is mainly caused by T_1, T_2 and $1/\gamma\Delta B$ (inhomogeneities of

the external magnetic flux density) [23,25]. Consequently, after applying the Fourier Transform (FT) to a NMR signal, a frequency distribution will be obtained. If $\gamma\Delta B >> 1/T_1 + 1/T_2$, the sample magnetic susceptibility is uniform. Considering that this frequency spectrum can be interpreted as a probability distribution of the magnetic flux density (that is, the amplitude represents the probability to find a given value within the sample volume), the most representative value of B is the expectation value of the distribution $E(B)$:

$$E(B) = E(\omega)/(\gamma). \quad (1)$$

In this equation, $E(\omega)$ is the expectation value of the frequency distribution. In addition, the magnetic flux density B depends on the magnetic permeability μ of the sample:

$$B = \mu H .$$

Here, H is the external magnetic field generated by the electromagnet (independently of the sample). Finally, the expectation value of external magnetic field can be obtained as:

$$E(H) = E(B)/\mu . \quad (2)$$

If phase detection of the NMR signal is used, the original signal induced at the coil of the NMR probe (at a frequency that equals the Larmor frequency) becomes mixed with a reference radio frequency (RF) ω_0 of constant amplitude and frequency, which is the same frequency used to excite the spin-system. The output down-converted FID (detected NMR signal) will have a frequency $\omega_d = |\omega - \omega_0|$ and will be modulated in amplitude according to the envolvent of the FID. When the excitation (and mixing reference) frequency ω_0 equals the precession frequency ω of the spins (Larmor frequency), it is said that the experiment is being made "on resonance". In this case the phase-detected FID will consist only in its envolvent. Otherwise, it will consist in an oscillatory decay signal with an audio-frequency $\omega_d \neq 0$ (equivalent to the off-resonance). This signal is represented by a frequency distribution instead of a single frequency. From the experiments we learn that the resonance condition is met if the RF excitation (and mixing reference) frequency matches the most probable value of the magnetic flux density distribution. Consequently, it is possible to measure $E(B)$ through a NMR measurement.

c) Measurand

The FT of the NMR signal represents a probability density distribution of the nuclear frequency precessions within the sample volume. Hence, considering the frequency ω as a random variable, it can be treated as a probability density function (PDF) $g_B(\omega)$ [26]. Therefore, the best estimation of

ω is the expectation value $E(\omega)$, which we define here as $E(\omega)=\omega_E$:

$$\omega_E = \int_{-\infty}^{\infty} \omega g_B(\omega) d\omega . \qquad (3)$$

Following equation (1), the magnetic flux density is $|E(B)| = |(\omega_E / \gamma)|$ and the generated external magnetic field is $|E(H)| = |(\omega_E / \mu\gamma)|$. That is, the best expectation of the magnetic field magnitude can be determined through the expectation value of the detected NMR signal frequency, the magnetic permeability of the sample μ and the gyromagnetic ratio γ. These last two magnitudes were already measured by different laboratories and can be obtained from the literature.

EXPERIMENTAL

Two measurement methods will be presented. Both cases comply with the conditions stated for the measurement model. Consequently, the condition $\gamma\Delta B >> 1/T_1 + 1/T_2$ is one of the main differences with the work of Xiang Fei et al. [16]. Here we focus on the shape of the FT of the NMR signal. In both methods, the proton NMR signal acquisition procedure is the same.

Signal acquisition

The most straightforward experiments to obtain the NMR signal are the acquisition of a FID and the Hahn ECHO [27]. In the FID experiment, the simplest possible experiment in pulse NMR, the signal is acquired immediately after a single RF pulse (a hard $\pi/2$ pulse). However, due to receiver saturation after the hard RF pulse, part of the FID signal is lost during the "dead-time" of the acquisition. The hardware can be optimized to minimize this dead-time, but there always be a signal loss due to this effect. As a consequence, part of the information contained at the beginning of the FID signal becomes lost. Moreover, the FID signal has no defined symmetry. It will be shown that this situation is not desirable if a Discrete Fourier Transform (DFT) would be used. On the other hand, in the two-pulse Hahn ECHO experiment, RF pulse imperfections effects can be minimized after a calibration of the pulse sequence [28]. The main advantage of using an ECHO signal instead of a FID relays in the fact that the signal preserves all the information. It is closer to be symmetric (particularly at low-resolution), and it is acquired far away from the second RF pulse (and consequently not being affected by the receiver dead-time). These facts are reflected in a minor or null loss of information and a much lower distortion of the DFT signal.

Robustness of the ECHO signal under DFT

The DFT applied to a FID signal present the same problem observed in the sampling during a finite time window of a periodic function. It is clear today that conventional DFT do not work properly for discontinuous functions [29,30]. The discontinuity (at the beginning of the signal in the case of the FID) is similar to a truncation due to a finite acquisition window. The consequence in applying the DFT in these cases is that a "spectral leakage" will affect the transformed signal. It is a mere consequence arising from the discontinuity of the sampled function and not related with the sampling properties, and affects the entire basis set of the spectrum [31]. This leakage provokes a bias for both the amplitude and position of a harmonic component, being more relevant for those portions of the FID having smaller amplitude (that is, it mainly affects the long-lasting components of the FID). This last point can be completely mitigated by acquiring the Hahn Echo instead of the FID. In addition, the transformed signal is affected by the broadband noise spectrum and eventual noise components within the bandwidth of the acquired window, which affects both the echo and the FID in a similar extent (effect that can be minimized by a proper filtering).

Although non-conventional algorithms can be used for discontinuous functions (Conjugate-gradient FFT, interpolation methods, etc.), the possibility to acquire a symmetric signal by using a two-pulse NMR sequence in our case simplifies the problem by allowing the use of well-tested conventional algorithms. The poor accuracy of the conventional DFT applied to the FID can be easily illustrated by considering the behavior of a data set $S(t_i)$ subjected to a transformation [32,33]. A simple way to do this it is to compare the inverse transformation $I(F(S(t_i)))$ of the FFT of the original data set, that is $F(S(t_i))$, with $S(t_i)$. The sum of the absolute value of this difference for each point of the data set will be called δ:

$$\delta = \sum_{i=1}^{N} \left| S(t_i) - I\left(F\left(S(t_i)\right)\right) \right|. \qquad (4)$$

If $\delta = 0$ (that is both data sets are coincident point by point), the signal is undistorted under a FFT. Consequently, there is no spectral leakage. The application of the conventional algorithm shows that in the case of the ECHO signal $\delta = 0$, while for the FID $\delta \neq 0$.

In summary, the DFT of the ECHO signal is the best estimation of the probability density distribution of a magnetic induction field B as observed in an NMR experiment. Therefore, the Hahn-ECHO sequence (see Figure 1) is used with the parameters shown in Table 1.

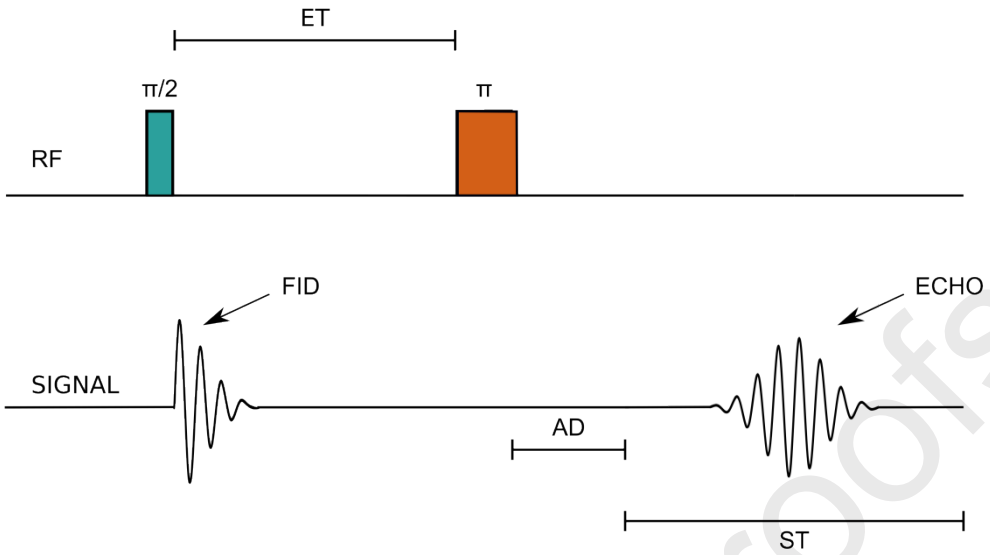

Figure 1: Hahn ECHO sequence with each parameter used in the experiment. See text for details.

In Table 1, ST represents the acquisition time window, AD is the acquisition delay defined as the time between the end of the second RF pulse and the beginning of the acquisition window, ET (ECHO time) is the time between the end of the first RF pulse and the beginning of the second one and finally, NP represents the number of acquisition points. These parameters are chosen as the result of an optimization of SNR (signal-to-noise ratio) and to sample the same quantity of zeros at both time and frequency domains.

ST	(7.680 ±0. 001) ms
AD	(1.500±0. 001) ms
ET	(4.000±0. 001) ms
NP	128

Table 1: Parameters of the Hahn-ECHO sequence. See text for details.

Indirect method

The DFT of the acquired ECHO is a discrete probability density function (DPDF), $g_B(\omega_i)$, where the basis set ω_i ranges from i = 1 to 128. In this method a fitting is proposed to obtain the best estimation of the probability density function PDF or $g_B(\omega)$. Once this function has been obtained,

the expectation value can be calculated using well established methods. The proposed fitting method is a linear combination of symmetric distributions. In particular, Gauss distributions are the functions that best fit our experiments.

A criterion is established to determine the quantity of Gaussian functions used to fit $g_B(\omega)$. If M signals are acquired, after the FFT there will be the same quantity of DPDFs, $g_{Bj}(\omega_i)$, where g_{Bj} corresponds to the j^{st} acquisition. Therefore, we may define a mean $<g_{Bj}(\omega_i)>$ with its associated standard deviation $\sigma_B(\omega_i)$. On the other hand, for each j-DPDF or $g_{Bj}(\omega_i)$, we may define a Γ_{jk} as the linear combination of Gaussian functions that best fit the discrete function:

$$\Gamma_{jk} = c_{j1}G_{j1} + c_{j2}G_{j2} + ... + c_{jk}G_{jk}\ , \qquad (5)$$

where the G_{jk} represent the Gauss distribution set with the corresponding weighting parameters c_{jk}.

The key point here is to find the optimal fitting by considering that the needed precision is given by the intrinsic variations between different acquisitions. Fitting $g_{Bj}(\omega_i)$ with a higher accuracy than the stability of the system, will have no impact on the final result. Hence, the optimization criterion is the following (for each value of i):

$$\left(\Gamma_{jk}(\omega_i) - g_{B_j}(\omega_i)\right)^2 < {\sigma_B}^2(\omega_i)\,. \qquad (6)$$

For the acquired signals we found that $k = 3$ is enough to fulfill this condition, that is, a linear combination of 3 Gaussian distributions is enough to fit our DPDFs (see Figure 2).

The expectation value ω_{Ej} is calculated for each of the M acquired signals (i.e., j runs from 1 to M). The most representative value obtained from the M samples is the mean value $\langle\omega_E\rangle$. The corresponding uncertainty is the experimental standard deviation of the mean σ_E multiplied by a coverage factor of 95%, where these quantities are defined by:

$$\langle\omega_E\rangle = \frac{1}{M}\sum_{j=1}^{M}\omega_{Ej}\ , \qquad \Delta\langle\omega_E\rangle = t_{\alpha/2,\upsilon}\frac{\sigma_E}{\sqrt{M}} \qquad (7)$$

and

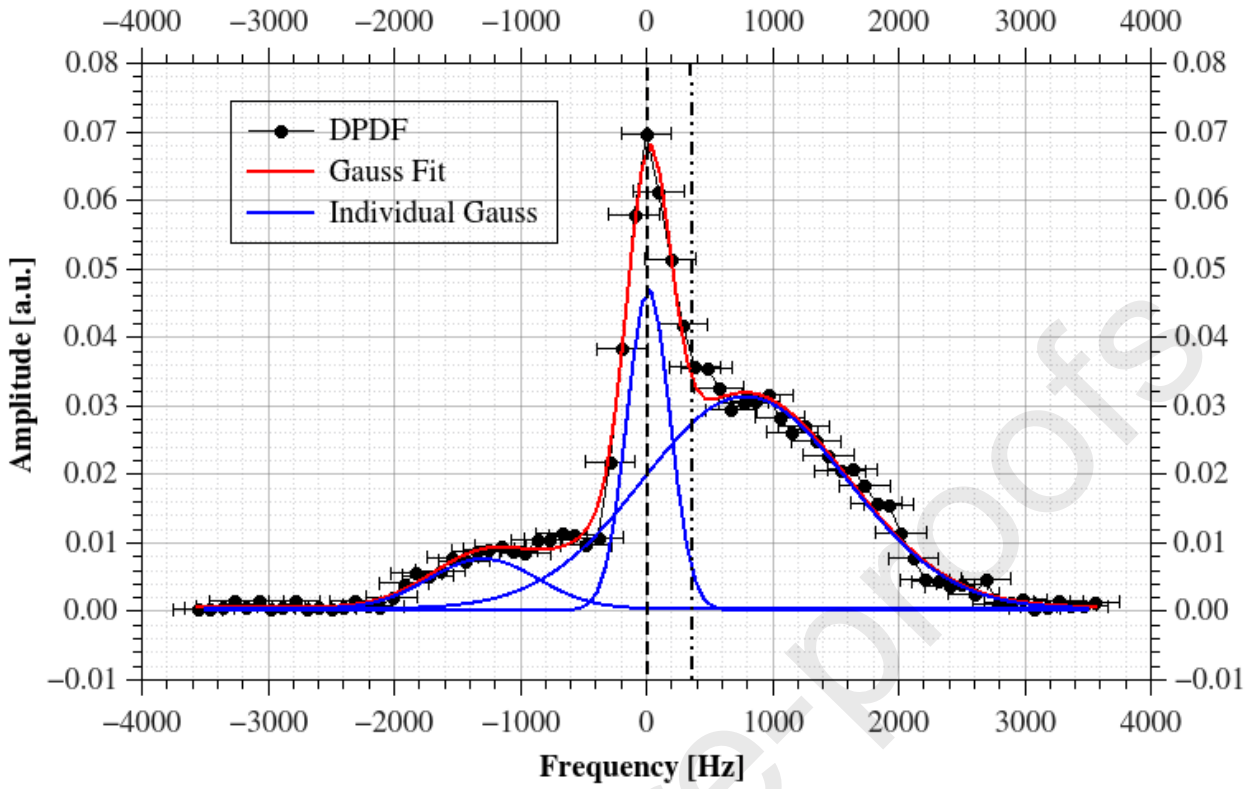

Figure 2: DFFT of one acquisition with its fitting curve. The red curve is the sum of the blue curves (single Gaussian functions). The uncertainty associated for each black point is the uncertainty of the RF synthesizer. The solid black line indicates the frequency $\omega_{Mj} \cong 0Hz$ associated to the point of maximum amplitude. The dotted black line is located at the expectation value of the frequency (see equation (3)): $\omega_{Ej} \cong 390Hz$.

$$\sigma_E^{\,2} = \frac{1}{M-1}\sum_{j=1}^{M}\left(\omega_{Ej} - \langle\omega_E\rangle\right)^2. \qquad (8)$$

Here $t_{\alpha/2,\nu}$ is a coverage factor determined by the t-Student table and $\Delta\langle\omega_E\rangle$ is the uncertainty associated to $\langle\omega_E\rangle$ (by a coverage factor of 95%).

a) Measurement system

The measuring system is composed of a Stelar (Mede, Italy) console and a Bruker (Karlsruhe, Germany) electromagnet model B-E10. The magnetic field strength can be adjusted by the variation of the electric current supplied by the power source and/or the gap between the polar faces of the magnet. The power supply is a Heinzinger (Rosenheim, Germany) Tns-125-2500. The RF pulses are amplified by a 1 KW power Kalmus (Bothell, USA) LP-1000 transmitter. Figure 3 shows a schematic diagram of the instrument.

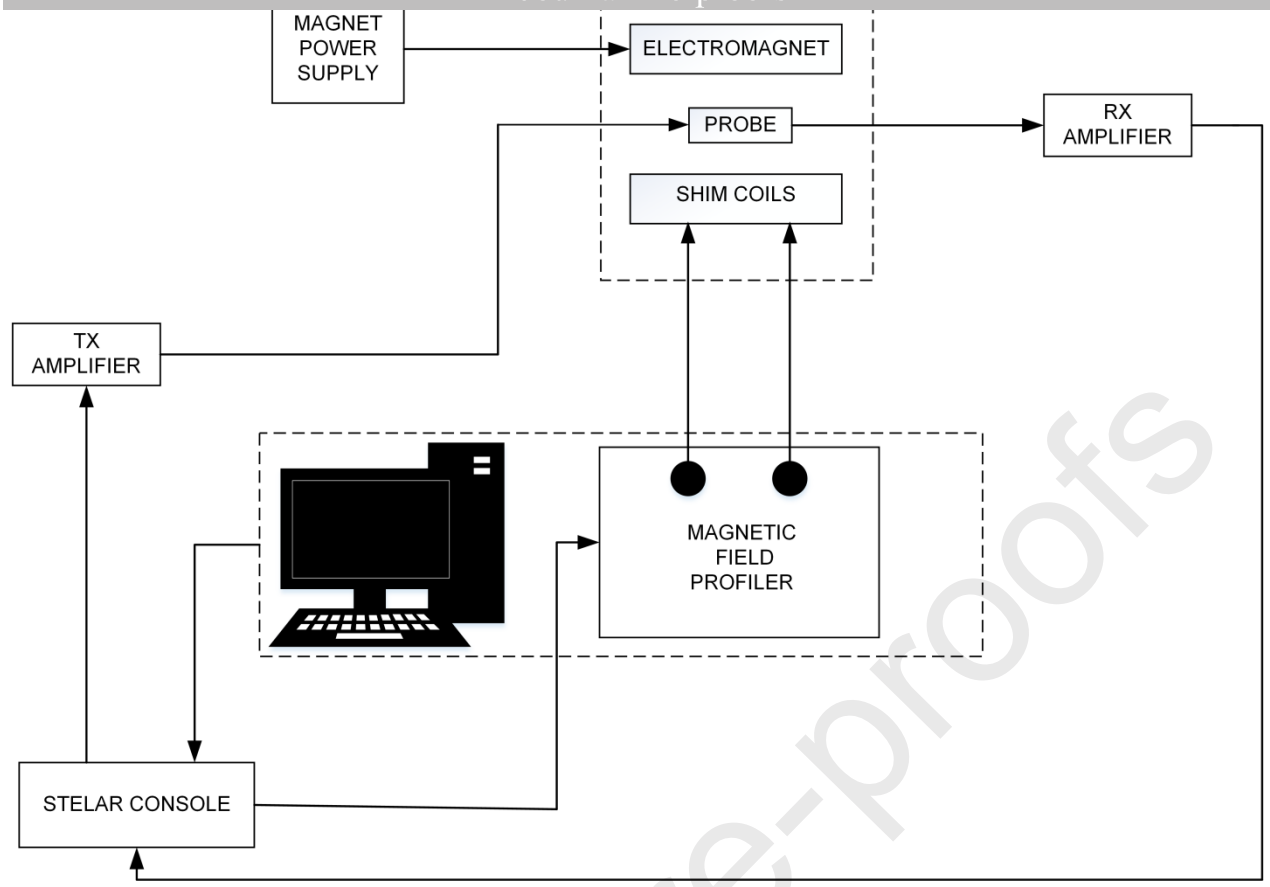

Figure 3: Block diagram of the NMR equipment. Tx represent the RF transmitter and Rx the signal amplifier. The Console generates the RF pulses and acquires the signal.

The system is based on a variable gap electromagnet that allows measuring selected points of a magnetic field calibration curve by setting different electromagnet currents. A specific NMR probe is optimized for each corresponding Larmor frequency. A special sample holder was engineered for the calibration of Hall-effect sensors and probes. The volume of the NMR sample must be bigger than the greatest active area of the Hall sensor to be calibrated. However, as the sample holder size is directly related with the magnetic field uncertainty, it should be as small as possible. As a compromise solution between these requirements, the size of the sample holder was set to 12.12mm x 7.80mm x 1.26mm (±0.08mm each). The used sample was pure water with a conductivity of $18 M\Omega / cm$ measured at room temperature, obtained from an Apema (Buenos Aires, Argentina) Osmoion 5a milli-Q purification system.

b) Results

The experiment was repeated 21 times to check repeatability. In this way we consider all the uncertainties in only one statistic uncertainty (Type A). A DFFT and the subsequent fitting were done for each of the individual acquisitions $g_{Bj}(\omega_i)$, and then each ω_{Ej} and ω_{Mj} evaluated. Finally, the

most representative value with its standard deviation and $\langle\omega_M\rangle$ are obtained:

$$\begin{aligned} \langle\omega_E\rangle &= (330 \pm 60)\,Hz \\ \sigma_E &= (28 \pm 4)Hz \\ \langle\omega_M\rangle &= (-20 \pm 90)\,Hz \end{aligned} \qquad (9)$$

All the uncertainties are expressed within a coverage factor of 95% considering a Student distribution. These results are indistinguishable from the values obtained in the fitting of each $g_{Bj}(\omega_i)$. This fact shows that the method is robust. The mean expectation value $\langle\omega_E\rangle$ is clearly distinguishable from $\langle\omega_M\rangle$ due to the asymmetry of the distribution. However, $\langle\omega_M\rangle$ is indistinguishable from zero. The NMR system frequency was ω = 19490000 Hz. This is the frequency associated with the zero of the distribution. Hence, the real value of the expectation value of the frequency is:

$$\langle\omega_E\rangle = (19490330 \pm 60)\,Hz \text{, with } \Delta\langle\omega_E\rangle / \langle\omega_E\rangle = 3ppm\,. \qquad (10)$$

The reference RF frequency ω = 19490000 Hz was calibrated by the INTI (Argentinian Institute of Industrial Technology). χ and γ were obtained from the literature [34,35]:

$$\gamma = (42577.480 \pm 0.001)Hz/mT \text{, where } \Delta\gamma/\gamma = 0.02\,ppm\,. \qquad (11)$$

In order to establish the uncertainty of χ, a temperature range from 15ºC to 25ºC was considered. μ was calculated as $\mu = (1+\chi)$, with $\chi = (-0.7220 \pm 0.0005).10^{-6}$:

$$\mu = (0.9999992780 \pm 0.0000000005),$$

with $\Delta\mu/\mu = 0.0005ppm$.

Finally, from eq. (2) $E(H)$ can be obtained:

$$E(H) = (457.762 \pm 0.001)\,mT \text{, where } \Delta E(H)/E(H) = 3\,ppm\,. \qquad (13)$$

As it can be seen, the uncertainty of $E(H)$ is dominated by the uncertainty of $\langle\omega_E\rangle$.

Direct method

When the RF frequency transmitted to the sample coincides with the most probable frequency ω_M in a NMR experiment, the magnetic resonance phenomenon manifests. We refer to this particular frequency as "resonance frequency" $\omega_0{}^0$. Here we will use the fact that this frequency can be measured. Later, we can obtain ω_E from $\omega_0{}^0$. However, if the distribution resulting from the DFT of the NMR signal turns asymmetric, ω_E may be distinguishable from $\omega_0{}^0$ and ω_M. A possible solution consists in adding correcting magnetic fields that affect the homogeneity of the magnetic field across the sample, in order to obtain a symmetric DFT signal.

In this work we discuss the use of a compensation system (we call it MFP or "Magnetic Field Profiler") to obtain a symmetric distribution. The experimental situation has already been described in an earlier publication [36]. We consider a distribution $g_{Bj}(\omega_i)$ to be symmetric when it can be properly fitted with only one Gaussian function After that, $\langle \omega_E \rangle$ is determined from several signals, and it can be compared with $\omega_0{}^0$. Once both values are indistinguishable, a measurement of $\langle \omega_E \rangle$ can be realized by measuring the resonance frequency in the same conditions, without the need of any fitting. In this case, the uncertainty of the resonance frequency is also determined by statistics. Different steps of the procedure are described in the next section.

a) MFP Compensation system: hardware description

The measurement system is the same as described before, with the addition of the MFP hardware. The control of the magnetic field spatial dependence was implemented using an improved version of the hardware presented in reference [36]. A block diagram of this device is shown in Figure 4.

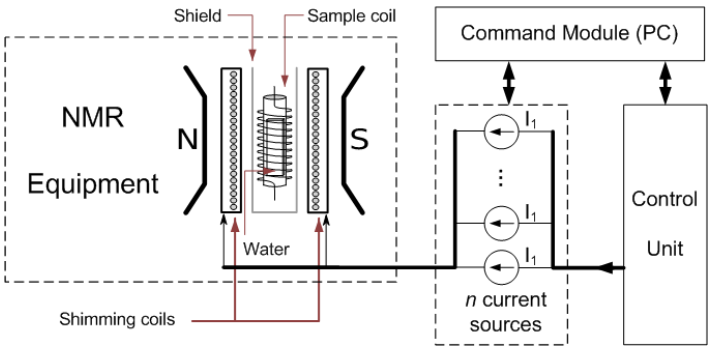

Figure 4: Block diagram of the Magnetic Field Profiler (MFP) system.

The MFP system consists in a set of coils that generates the compensating magnetic fields and their associated current sources (Figure 4). The system uses an algorithm to optimize the currents driving the set of coils which runs continuously until the DFFT of the NMR signals show-up a symmetric distribution. In [36] a generic coil configuration was used just to test the concept. In this work, the correcting coils were specifically designed after mapping the magnetic field of the NMR instrument. With this purpose, a small NMR sample (volume of 0.15cm^3) was moved within the magnetic field volume to be calibrated, using a special sample (probe) positioning system (see Figure 5).

Based on the information of Figure 5, the selected coil configuration corresponds to a T20 shim coil as discussed in reference [37]. Figure 6 shows a coil arrangement which will be called **CA1**. A similar coil set called **CA2** is located in front of **CA1** (each parallel to a pole face of the magnet). Coil **#1** of **CA1** is connected in anti-Helmholtz configuration with coil **#2** of **CA2**; coil **#2** of **CA1** is connected in anti-Helmholtz configuration with coil **#1** of **CA2**. Coils **#3a** and **#3b** (in series) of **CA1** are connected in anti-Helmholtz configuration with coils **#3a** and **#3b** of **CA2** (also in series). Finally, a similar configuration applies to coils **#4a** and **#4b** of **CA1:** connected with #**4a** and **#4b** of **CA2,** each pair connected in series**.** In this way, the MFP device has four shimming channels, each of them connected to a current source which is managed by the system controller that executes the control algorithm tasks. The compensation coils generate a magnetic field profile that is additive with the NMR Instrument Zeeman field, resulting in a more homogeneous magnetic field as compared to the results obtained in [36].

In principle the optimal current values can be found after an exhaustive search of all the possible current combinations. However, this is not practical because of the time that this procedure would take. For example, if there are four compensation coils, and each current is controlled with an 8 bits digital power source, there are 256^4 possible current values. Assuming that it takes 1ms among NMR experiments of different current sets, it would take 1193 hours to go over the whole search space, which is clearly unpractical. A successive approximation method was used in reference [36] for the optimization of the current intensities. The step by step correction of each current value was based on the optimization of a discriminant function (f_d), whose terms were obtained from a statistical characterization of the FID signal. f_d tend to a minimum as the FID approach a pre-defined mono-exponential decay, theoretically corresponding to the target magnetic field homogeneity. However, a main drawback of this algorithm was the poor immunity to noise, thus affecting the convergence of the optimization.

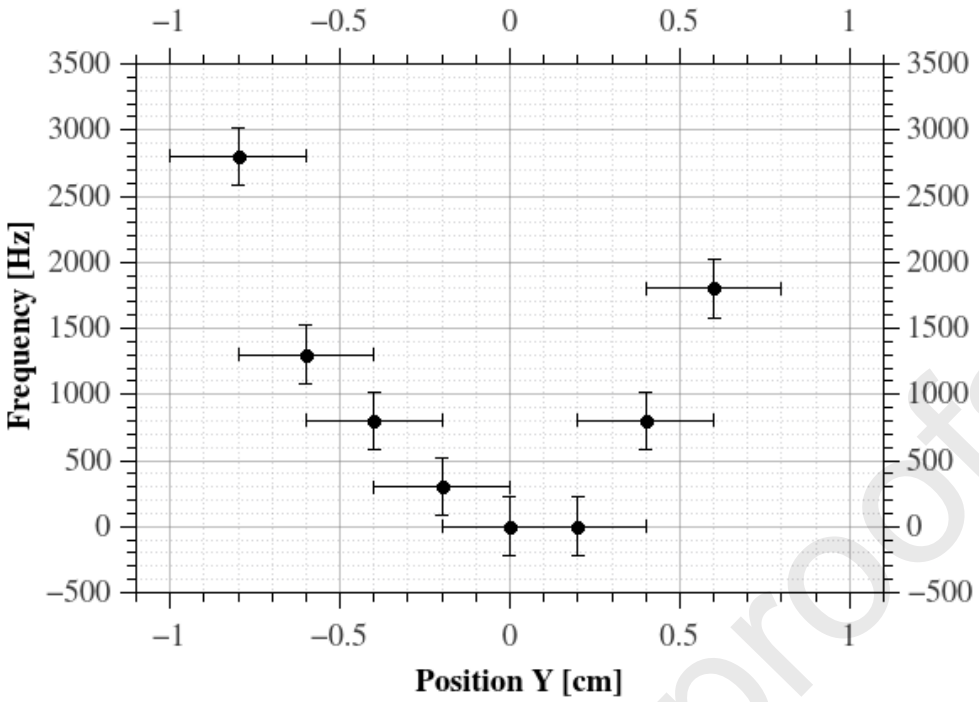

Figure 5: field map obtained in y direction within the volume space where the magnetic field induction field needs to be calibrated. The magnetic induction field increase outside the center of the magnet (the x,y plane is parallel to the polar faces of the magnet, and the z axis coincides with the direction of the generated Zeeman magnetic field). The uncertainty associated to the position was determined by the size of the sample and the precision of the sample positioning system. The frequency uncertainty was determined by statistics with a 95% of coverage factor.

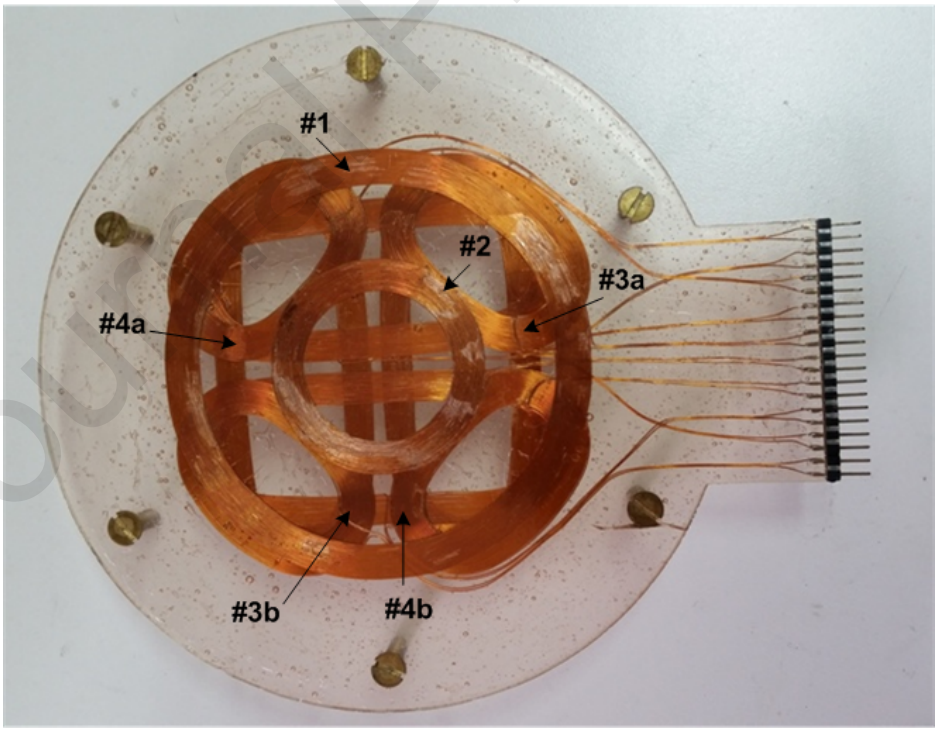

Figure 6: The shimming coil arrangement consists of two set of coils like the image of this figure, placed in parallel to each pole-face of the electromagnet. See text for a detail of coils interconnections with the respective powering channels.

In this work we propose an alternative algorithm based on the FT of the ECHO signal (Figure 7). Now the convergence criteria are:

a) Maximization of the ratio B_{max}/a_m (where B_{max} is normalized to 1).

b) The ECHO Fourier Transform should be as close as possible to a Gaussian function.

Consequently, we can redefine the discriminant function f_d as:

$$f_d = k_1\, a_m + k_2 s + k_3 T_e\ , \qquad (14)$$

where k_1, k_2 y k_3 are configuration parameters, a_m is the ECHO FFT width at half amplitude m, s is a symmetry parameter and T_e is the total length of the ECHO signal (see Figure 7).

$$a_m = \left| f_2 - f_1 \right|\ , \qquad (15)$$

where f_1 and f_2, are the frequency values corresponding to the intersections between the ECO FFT and the constant m. The s parameter is a measure of symmetry defined as:

$$s = \omega_M - \omega_E\ . \qquad (16)$$

b) Results

Figure 8 shows the probability density distribution of the magnetic field corresponding to an optimized magnetic flux density using the MFP device. Now the distribution can be fitted using a unique Gaussian function.

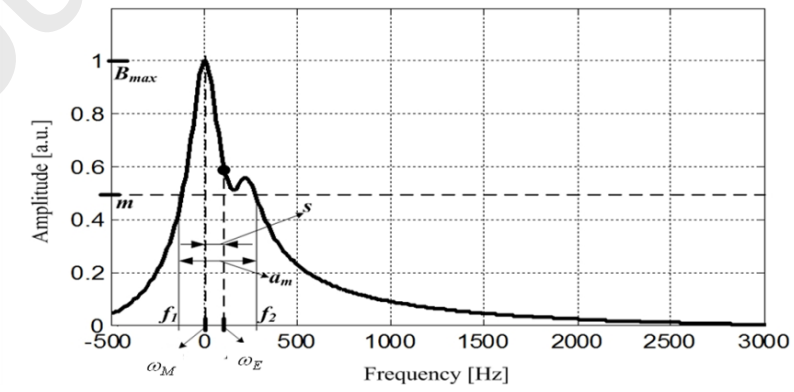

Figure 7: f_d parameters used in this work. Optimization parameters are measured from the frequency distribution curve (FFT of the ECHO signal). Here B_{max} corresponds to the maximum value; m is the half-maximum, a_m the bandwidth at half-maximum (f_2-f_1), and s is a parameter reflecting the symmetry of the distribution.

Like in the indirect method, the experiment was repeated 21 times. Therefore, $\langle \omega_E \rangle$ and σ_E were calculated:

$$\langle \omega_E \rangle = (50 \pm 80)\, Hz\,, \qquad \sigma_E = (37 \pm 4) Hz\,. \tag{17}$$

In the symmetric case $\langle \omega_E \rangle = \langle \omega_M \rangle$ and they are indistinguishable from zero. Hence, $\langle \omega_E \rangle$ is indistinguishable from $\omega_0{}^0$. Therefore, it is possible to obtain the value of $\langle \omega_E \rangle$ by a direct measure of $\omega_0{}^0$.

$$\omega_0^0 = (19503000 \pm 200)\, Hz\,, \text{ with } \Delta\omega_0^0 / \omega_0^0 = 10\, ppm\,. \tag{18}$$

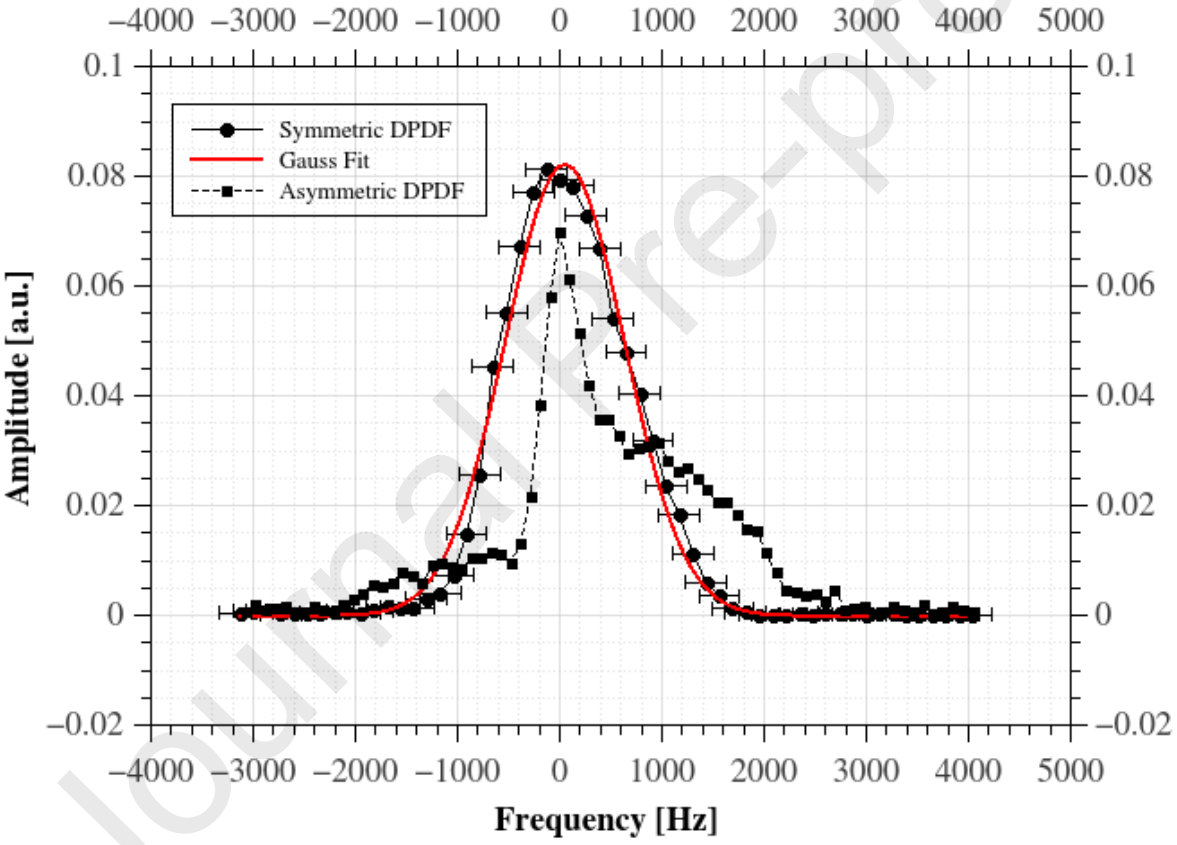

Figure 8: Symmetric distribution with one Gaussian fitting and the asymmetric uncompensated distribution.

The uncertainty of $\omega_0{}^0$ was determined by statistics after measuring the resonance frequency 64 times. The measured resonance frequency is slightly higher than the corresponding to the indirect method due to the additional correcting field added by the compensation system. Finally, with $\omega_0{}^0$ and the same values of χ and γ used in the indirect method, we get:

$E(H) = (458.059 \pm 0.005)mT$, where $\Delta E(H)/E(H) = 10\,ppm$ (19)

CONCLUSIONS

The magnetic flux density was determined using the NMR phenomenon within a given volume in order to use it as a calibrating reference for magnetic metrology. Two different experimental procedures were analyzed. Both cases allowed reference magnetic flux densities with a few ppm of uncertainty, within a volume of about 0.1cm^3:

1- Indirect method: $E(H) = (457.762 \pm 0.001)mT$

2- Direct method: $E(H) = (458.059 \pm 0.005)mT$

While the indirect method requires a higher amount of data processing, the direct method is faster and simpler. The proposed MFP control algorithm is based on parameters that can be directly extracted from the FFT of the ECHO signal. This method showed a much higher robustness than the previously used based on statistical signal characterization [38]. The key feature relays in the higher immunity to noise of the FFT. The MFP system allows symmetrizing and optimizing the FFT of the ECHO signal through a direct hardware-intervention that corrects the magnetic flux density homogeneity with the volume of interest. Although in the example treated in this manuscript it turned out that the resulting uncertainty is smaller for the indirect method (that is, without the need of additional hardware), the main advantage of the last relays in that it can always be improved by refining both the hardware and the convergence algorithm. By a precision mapping of the magnetic field to be corrected, adequate specific correcting-coils can be implemented. In addition, the number of channels can be increased. Consequently, the precision of the last method is only limited by the hardware performance.

Finally, both methods meet all requirements for the design of NMR primary magnetic flux density standards, vastly superior to Helmholtz-coil based set-ups. The methods here described can be implemented in any NMR apparatus, also in cases with permanent or superconducting magnets. The main advantage of the electromagnet is that several calibrating points can be optimized in the same instrument. Although not considered along this manuscript, it is felt strongly that the NMR methods here described represent an excellent option for the set-up of calibrating references of magnetic flux densities at an extremely competitive cost equation.

ACKNOWLEDGEMENTS

The authors acknowledge to Ing. Roberto Muñoz (Unidad Técnica Electrónica, INTI Centro Regional Córdoba) and to Dr. Clemar A. Schürrer (CEMETRO, Universidad Tecnológica Nacional, RFC) for fruitful discussions. Financial support from Secyt-UNC, CONICET and FONCYT is highly appreciated.

REFERENCES

[1]- Ruark, A. E., Peters, M. F., *Helmholtz Coils for Producing Uniform Magnetic Fields,* J. Opt. Soc. Am., 13 (1926), 205-212.

[2]-Trout S. R., *Use of Helmholtz Coils for Magnetic Measurements,* IEEE Trans. Magn. 24 (1988) 2108-2111.

[3]- Purcell E. M., *Helmholtz coils revisited*, Am. J. Phys. 57 (1989) 18-22.

[4]- Frix W. M., Karady G. G., Venetz B. A., *Comparison of calibration systems for magnetic field measurement equipment,* IEEE Trans. Power Deliv. 9 (1994) 100-108.

[5]- Crosser M. S., Scott S., Clark A., Wilt P. M., *On the magnetic field near the center of Helmhotz coils,* Rev. Sci. Instrum. 81 (2010) 084701.

[6]- Beiranvand R., *Effects of the Winding Cross-Section Shape on the Magnetic Field Uniformity of the High Field Circular Helmholtz Coil Systems*, IEEE Trans. Industrial Electron. 64 (2017) 7120-7131.

[7]- Geršak G., Humar J., Fefer D., *Calibration of a reference field coil by means of the NMR magnetometer and induction coils*, Elektrotehniški vestnik (Electrotech. Rev., Ljubljana) 68 (2001) 294-299.

[8]- Park P. G., Kim Y. G., Shifrin V. Ya., Khorev V. N., *Precise standard system for low dc magnetic field reproduction*, Rev. Sci. Instrum. 73 (2002) 3107-3111.

[9]- Périgo E. A., Martin R. V., *Magnetic Field and Gradient Standards Using Permanent Magnets: Design Considerations, Construction and Validation by Nuclear Magnetic Resonance*, IEEE Trans. Magn. 49 (2013) 4717-4720.

[10]- Dadydov V. V., Velichko E. N., Dudkin V. I., Karseev A. Yu., *A nutation nuclear-magnetic teslameter for measuring weak magnetic fields,* Meas. Tech. 57 (2014) 684-689. Translated from Metrologiya 5 (2014) 32-41.

[11]- Ulvr M., Kupec J., *Improvements to the NMR Method with Flowing Water at CMI*, IEEE Trans. Instrum. Meas. 67 (2018) 204-208.

[12]- Grech C., Avramidou R., Beaumont A., Buzio M., Sammut N., Thembart J., *Metrological Characterization of Nuclear Magnetic Resonance Markers for Real-Time Field Control of the CERN ELENA Ring Dipoles*, IEEE Sens. J. 18 (2018) 5826-5833.

[13]- Abragam A., *The Principles of Nuclear Magnetisn,* Claredon Press, Oxford (1961).

[14]- Williams E. R., Jones G. R., Sheng Ye R. L., Hitoshi S., Olsen T., Phillips W. D., Layer H. P., *A Low Field Determination of the Proton Gyromagnetic Ratio in Water,* IEEE Trans. Instrum. Meas. 38 (1989) 233-237.

[15]- Woo B. C., Kim C. G., Park P. G., Kim C. S., Shifrin V. Y., *Low Magnetic Field Measurement by a Separated NMR Detector Using Flowing Water*, IEEE Trans. Magn. 33 (1997) 4345-4348.

[16]- Fei X., Hughes V. W., Prig R., *Precision measurement of the magnetic field in terms of the free-proton NMR frequency*, Nucl. Instr. Meth. Phys. Res. A 394 (1997) 349-356.

[17]- Garcon A. et al, *The cosmic axion spin precession experiment (CASPEr): a dark-matter search with nuclear magnetic resonance,* Quantum Sci. Technol. 3 (2018) 014008.

[18]- Petley B. W., *Time and Frequency in Fundamental Metrology*, Proceed. IEEE 79 (1991) 1070-1076.

[19]- Beguš S., Fefer D., *An absorption-type proton NMR magnetometer for measuring low magnetic fields*, Meas. Sci. Technol. 18 (2007) 901-906.

[20]- Dong H., Liu H., Ge J., Zhiwen Y., Zhizhuo Z., *A High-Precision Frequency Measurement Algorithm for FID Signal of Proton Magnetometer*, IEEE Trans. Instrum. Meas. 65 (2016) 898-904.

[21]- Bloch F., Hansen W. W., Packard M., *Nuclear induction*, Phys. Rev. 69 (1946) 127-127.

[22]- Purcel E. M., Torrey H. C., Pound R. V., *Resonance Absorption by Nuclear Magnetic Moments in a Solid*, Phys. Rev. **69** (1946) 37-38.

[23]- Fukushima E. et al, *Experimental Pulse NMR: A Nuts and Bolts Approach*, Addison-Wesley, Massachusetts (1993).

[24]- Maudsley A. A., Simon H. E., Hilal S. K., *Magnetic field measurement by NMR imaging*, J. Phys. E: Sci. Instrum.17 (1984) 216-220.

[25]- Bloembergen N., Purcell E. M., Pound R. V., *Relaxation Effects in Nuclear Magnetic Resonance Absorption*, Phys. Rev. 73 (1948) 679-712.

[26]- Joint Committee for Guides in Metrology, *Evaluation of measurement data* — Supplement 1, "Guide to the expression of uncertainty in measurement-Propagation of distributions using a Monte Carlo Method" JCGM 101, (2008).

[27]- Hahn E. L., *Spin Echoes*, Phys. Rev. 80 (1950) 580-594.

[28]- Vold R. L., Vold R. R., Simon H. E., *Errors in Measurements of Transverse Relaxation Rates*, J. Magn. Reson. 11 (1973) 283-298.

[29]- Fan G.-X., Liu Q. H., *Fast Fourier Transform for Discontinuous Functions*, IEEE Trans. Antennas Propag. 52 (2004) 461-465.

[30]- Liu Y., Nie Z., Liu Q. H., *DIFFT: A Fast and Accurate Algorithm for Fourier Transform Integrals of Discontinuous Functions*, IEEE Microw. Wirel. Co. 18 (2008) 716-718.

[31]- Harris F. J., *On the Use of Windows for Harmonic Analysis with the Discrete Fourier Transform*, Proceed. IEEE 66 (1978) 51-83.

[32]- Kotyk J. J., Hoffman N. G., Hutton W. C., *Comparison of Fourier and Bayesian Analysis of NMR Signals I. Well-Separated Resonances (The Single-Frequency Case)*, J. Magn. Reson. 98 (1992) 483-500.

[33]- Kotyk J. J. et al., *II. Examination of Truncated Free Induction Decay NMR Data*, J. Magn. Reson. Series A 116 (1995) 1-9.

[34]- Cini R., Torrini M., *Temperature Dependence of the Magnetic Susceptibility of Water*, J. Chem. Phys. 49 (1968) 2826-2830.

[35]- https://www.physics.nist.gov/cgi-bin/cuu/Value?gammap

[36]- Segnorile H. H., Forte G. O., Farrher G. D., Anoardo E., *NMR-SSC Magnetic Field Profiler Applied to Magnetic Field Shimming*, IEEE Latin America Trans. 11 (2013) 257-262.

[37]- Liu W., Tang X., Zu D., *A Novel Target-Field Approach to Design Bi-Planar Shim Coils for Permanent-Magnet MRI*, Concepts Magn. Reson. 37B (2010) 29–38.

[38]- Hirsh H. L., *Statistical Signal Characterization*, Artech House, Boston (1991).

The authors declare to have no conflict of interest and no financial gain concerning the content of this manuscript.

- The role of the magnetic field inhomogeneity in NMR as a calibrating reference for magnetic metrology is discussed.
- Two different approaches to treat this aspect are presented.
- 1- A method based on the analysis of the Fourier Transform of the NMR ECHO signal.
- 2- A method including additional hardware (Magnetic Field Profiler or MFP) to compensate for magnetic field inhomogeneity.
- Both methods are compared with real measurements.

Conflict of Interest and Authorship Conformation Form

Please check the following as appropriate:

X All authors have participated in (a) conception and design, or analysis and interpretation of the data; (b) drafting the article or revising it critically for important intellectual content; and (c) approval of the final version.

X This manuscript has not been submitted to, nor is under review at, another journal or other publishing venue.

X The authors have no affiliation with any organization with a direct or indirect financial interest in the subject matter discussed in the manuscript